

NUMERICAL SIMULATIONS OF THE LONG RECIRCULATION BUBBLES FORMED IN INCOMPRESSIBLE AERODYNAMIC FLOWS OVER THIN FLAT PLATES AT SHALLOW INCIDENCE

Luiz Eduardo Bittencourt Sampaio

Dept. Mechanical Eng. – PUC/Rio, R. Marques de Sao Vicente 225 – Gávea, 22453-900 Rio de Janeiro, RJ, Brasil
luizebs@mec.puc-rio.br

Angela Ourivio Nieckele

Dept. Mechanical Eng. – PUC/Rio, R. Marques de Sao Vicente 225 – Gávea, 22453-900 Rio de Janeiro, RJ, Brasil
nieckele@mec.puc-rio.br

Margot Gerritsen

Dept. Mechanical Eng. – Stanford University, Stanford, CA, USA
margot.gerritsen@stanford.edu

Steve Collie

Dept. Mechanical Eng. – Stanford University, Stanford, CA, USA
steve.collie@gmail.com

Abstract. Aerodynamic flows around thin airfoil or membranes has experienced increasing attention from the industry and research institutions lately, and are prone to present complex structures, including geometry-induced separation of the boundary layer, shear layer transition to turbulent behavior, reattachment, relaminarization of the boundary layer, and formation of secondary recirculation bubbles. The particular case of a thin flat plate at 1 degree incidence and high Reynolds number (213000) is a good representative of this class of flows, and is studied in this paper using two different numerical approaches - Reynolds Average Navier-Stokes and Large-Eddy Simulations (LES), for which a mixed numerical scheme is implemented using the freely available open source CFD framework from OpenFOAM. The methodologies are compared to each other and to the available experimental data. LES is shown to better capture the complex structures, in contrast to RANS's intrinsic inability to deal with the strong anisotropy presented by the long and thin recirculation bubbles, observed in this kind of geometry. A physical insight on this complex and important class of flows is also presented, using the extensive amount of data provided by the numerical simulation, which encompass time evolution of most of the energy-containing vortical structures.

Keywords. thin flat plate, shallow incidence, turbulence, Large-Eddy Simulations

1. Introduction

Experimental investigations (Gault, 1955 and Crompton, 2001) of incompressible aerodynamic flows have shown that recirculation bubbles of different characteristics may be formed close to the leading edge of airfoils, depending on the geometry, incidence angle and Reynolds number. While short bubbles are commonly found in regular airfoils, resulting from an adverse pressure gradient (APG), longer and thinner recirculation structures, also known as "thin airfoil bubbles", are more often seen in thin plates and membranes, being their formation driven by a geometry-induced separation, rather than by an adverse pressure gradient one, as in the former case. Of paramount importance is the understanding of the differences between these two classes of recirculation bubbles, which are certainly not limited to length and thickness, but in fact the differences extend from the genesis mechanism to their influence on the behavior of the whole flow, including pressure distribution and reattachment point, just to cite a few.

Because of their adverse pressure gradient-induced separation, short bubbles formation usually involves a laminar boundary layer separation at some distance from the leading edge, followed by a shear layer transition to turbulence which, in its turn, helps mixing and reattachment. After reattachment, the fluid particles are split into those that follow the (now turbulent) boundary layer toward the trailing edge, and those that are driven back towards the leading edge, closing the recirculation structure. They usually span only 1- 2% of the chord, and don't alter significantly the pressure distribution, unless a burst is observed, which may cause transition to a longer bubble or even a complete stall. Therefore, the main reason for studying these structures is the importance of preventing the bursting and stalling phenomenon, rather than the understanding of their interaction with the rest of the flow.

Long bubbles, on the other hand, are formed after a separation of the boundary layer driven by an abruptness on the geometry, such as a knife-like leading edge on a thin plate, membrane or even thin airfoils (Fig. 1). Since the stagnation point for positive angle of attack is located in the lower surface of the plate, the fluid particles are unable to follow the abrupt curvature of the edge, as the inertial forces are dominant at high Reynolds numbers. The separation thus occurs right at the edge where the boundary layer is still laminar, and the separated layer - now a shear layer - will be developing towards a turbulent regime, after which the improved mixing helps curving the streamlines towards the

reattachment point. The fluid streams that go back towards the leading edge may still experience a relaminarization process, due to the now favorable pressure gradient formed between the reattachment point (higher pressure) and the minimum pressure point close to the center of the bubble. In its path toward the leading edge, the boundary layer, being laminar once again, is more prone to suffer a second separation, originating a secondary recirculation bubble, since from the minimum pressure point (center of the bubble) to the leading edge, another adverse pressure gradient is experienced. In contrast to regular curved airfoils where all the lift comes from the pressure distribution created by the streamlines curvatures, and where the short bubble, when present, causes unnoticeable disturbances, in the case of thin flat plate, most of the lift comes from the pressure developed inside the bubble to provide the centripetal force required to maintain the circular motion. It is also noteworthy that, due to the elongated aspect of these structures, strong anisotropy is expected in the turbulent statistics.



Figure 1. Physics of the Problem.

The alternative terminology "thin airfoil bubbles" to refer to long bubbles was given by Gault in 1957, and only recently, with thinner wing sections requirements imposed by the increasing aircraft speeds and advances in turbomachinery blades, this kind of structure has received more attention from the scientific community. Other important applications which would benefit from long bubble studies are yacht sails, parachute and paragliders. Among the most recent and complete experimental data available is the study performed by Crompton (2001), which focused on the simple thin flat plate geometry at shallow incidence, shown to be a very good representative and a strong benchmark case candidate for this class of flows.

Following the work of Crompton, numerical studies based on Reynolds Average Navier-Stokes methodology (RANS) from Collie et al. (2003) have pointed the inability of Reynolds Average models (RANS) to accurately predict the flow around thin flat plates and its complex structures. Since RANS models can not capture the strong anisotropy of this type of flow, Collie et al. (2003) suggested that further investigation was needed. To achieve this, at the present work, the Reynolds Average Navier-Stokes (RANS) and the Large-Eddy Simulation (LES) methodology were applied to the same thin flat plate test case, aiming a better understanding of the physics involved. In this work the opensource code OpenFOAM was used, with some minor modifications.

2. Reynolds Average Modeling

The Reynolds-averaged approach is based on decomposing the velocity as $\mathbf{u} = \bar{\mathbf{u}} + \mathbf{u}'$, where $\bar{\mathbf{u}}$ is the average velocity and \mathbf{u}' the velocity fluctuation. The average continuity and momentum equation (RANS), for a steady state incompressible flow is given by

$$\nabla \cdot \bar{\mathbf{u}} = 0 \quad ; \quad \nabla \cdot (\bar{\mathbf{u}} \bar{\mathbf{u}}) = -\nabla \left(\frac{p}{\rho} \right) + \frac{\mu}{\rho} \nabla^2 \bar{\mathbf{u}} + \nabla \cdot (-\overline{\mathbf{u}' \mathbf{u}'}) \quad (1)$$

where ρ is the density, μ is the molecular viscosity, p is the pressure. Equation (1) has the same form of the Navier-Stokes equation, but now it has an additional term, the turbulent Reynolds stress term, $-\overline{\mathbf{u}' \mathbf{u}'}$, representing the influence of the fluctuation on the average flow. In order to close Eq. (1), the turbulent Reynolds stress can be modeled based on the Boussinesq hypothesis as

$$-\overline{\mathbf{u}' \mathbf{u}'} = \nu_t (\nabla \bar{\mathbf{u}} + \nabla \bar{\mathbf{u}}^T) - \frac{2}{3} \kappa \delta \quad (2)$$

where κ is the turbulent kinetic energy and ν_t is the turbulence viscosity, which is defined in accordance with the κ - ω model of Wilcox (1988) as

$$\mu_t = \frac{\alpha^* \kappa}{\omega} \quad ; \quad \alpha^* = \left(\frac{0.008 + \mathbf{Re}_t/6}{1 + \mathbf{Re}_t/6} \right) \quad ; \quad \mathbf{Re}_t = \frac{\rho \kappa}{\mu \omega} \quad (3)$$

where κ and ω are obtained from their conservation equations

$$\nabla \cdot (\bar{\mathbf{u}} \kappa) = \nabla \cdot \left[\left(\frac{\mu}{\rho} + \frac{\nu_t}{\sigma_\kappa} \right) \nabla \kappa \right] + G_\kappa - \varepsilon \quad (4)$$

$$\nabla \cdot (\bar{\mathbf{u}} \omega) = \nabla \cdot \left[\left(\frac{\mu}{\rho} + \frac{\nu_t}{\sigma_\omega} \right) \nabla \omega \right] + \alpha \frac{\omega}{\kappa} G_\kappa - \beta f_\beta \omega^3 \quad (5)$$

$$G_\kappa = \nu_t S_{ij} S_{ij} \quad ; \quad f_\beta = \frac{1+70 \chi_\omega}{1+80 \chi_\omega} \quad ; \quad \chi_\omega = \left| \frac{\Omega_{ij} \Omega_{jk} S_{ki}}{(0.09 \omega)^3} \right| \quad ; \quad \alpha = \frac{0.52}{\alpha^*} \left(\frac{1/9 + \mathbf{Re}_t/2.95}{1 + \mathbf{Re}_t/2.95} \right) \quad (6)$$

$$S_{ij} = \frac{1}{2} \left(\frac{\partial \bar{u}_i}{\partial x_j} + \frac{\partial \bar{u}_j}{\partial x_i} \right) \quad \Omega_{ij} = \frac{1}{2} \left(\frac{\partial \bar{u}_i}{\partial x_j} - \frac{\partial \bar{u}_j}{\partial x_i} \right) \quad (7)$$

3. Large-Eddy Simulation Modeling

While RANS methodology uses a statistical or temporal filter to reduce the number of degrees of freedom of the original transport equations and all the turbulence is left to be modeled, Large-Eddy Simulation (LES) employs a spatial filtering operator to select the largest and most energetic structures to be computed, leaving only the small eddies to be modeled. Being those small eddies much less sensitive to the geometry and more isotropic, one can expect their modeling to be more universal when compared to RANS methodology.

The application of a filter operator $\langle \cdot \rangle$ into the incompressible Navier-Stokes and continuity equations, requires a two-step process to transform $\langle \nabla \cdot (\mathbf{u} \mathbf{u}) \rangle$ into $\nabla \cdot (\langle \mathbf{u} \rangle \langle \mathbf{u} \rangle)$. As a result two commutative errors are introduced. The first of one, defined as the commutative error, and hereby denoted by ϵ_{com} is a consequence of commuting the filtering process with a spatial derivative operator

$$\epsilon_{com} = \langle \nabla \cdot (\mathbf{u} \mathbf{u}) \rangle - \nabla \cdot (\langle \mathbf{u} \rangle \langle \mathbf{u} \rangle) \quad (8)$$

while the second which is a commutative product error, arises from commuting the filtering with the product operator. This second commutative error is commonly known as τ_{sgs} , the subgrid error or subgrid model (SGSM):

$$\tau_{sgs} = \langle \mathbf{u} \mathbf{u} \rangle - \langle \mathbf{u} \rangle \langle \mathbf{u} \rangle \quad (9)$$

It is common practice to ignore ϵ_{com} and concentrate more on the subgrid modeling. However, the awareness of its effect on the numerical scheme is extremely important when designing the mesh or when trying to prevent possible "checkered board" spatial instabilities that may arise. As shown by Germano (2000), depending on the filtering process, the effect of the commuting error may be equivalent to a spurious dissipation. In particular, when the mesh spacing increases in the upwind direction, the spurious viscosity coefficient associated with this effect may become too negative, causing numerical instabilities and eventually blowing out the solution. On the other hand, we cannot afford to use the same small mesh spacing required in the neighborhood of the leading edge all the way towards the inlet boundary.

This commutation error is found not only in LES, but also in RANS, since any discretization scheme can be seen as a more general filtering process. The fact that RANS models are not too affected by spatial instability problems is explained by the use of biased, highly dissipative numerical schemes, such as upwind. Large-Eddy Simulations generally cannot use such dissipative schemes, on the penalty of damping some important turbulence structure.

In the particular case of Finite Volume Method (FVM), the filtering operation may be conveniently confused with the volume integral over the control volume. Therefore, no further filtering is needed, and this process is said to be implicit, or embedded in the FVM, in which case it may be defined as:

$$\langle \varphi_i(t) \rangle = \frac{1}{\nabla_i} \int_{\nabla_i} \varphi(\mathbf{x}, t) d\mathcal{V} \quad (10)$$

where $\langle \varphi_i(t) \rangle$ is the value of the filtered variable located anywhere inside the i -th control volume, ∇_i , and $\varphi(\mathbf{x}, t)$ is the original field variable.

The filtered incompressible transport equations, for the filtered velocity $\langle \mathbf{u} \rangle$ can be written as

$$\nabla \cdot \langle \mathbf{u} \rangle = 0 \quad (11)$$

$$\frac{\partial \langle \mathbf{u} \rangle}{\partial t} + \nabla \cdot (\langle \mathbf{u} \rangle \langle \mathbf{u} \rangle) + \nabla \cdot \tau_{sgs} = - \nabla \left(\frac{\langle p \rangle}{\rho} \right) + \frac{\mu}{\rho} \nabla^2 \langle \mathbf{u} \rangle. \quad (12)$$

The vast majority of subgrid models (Sagaut, 2002), specially the eddy-viscosity ones, tries to capture only the forward energy cascade, where energy from the large eddies is transferred to small turbulent structures. In the continuous dynamic system, as found in real world, all this energy ends up being dissipated at very small scales, where laminar viscous dissipation becomes important. However, in a simulation environment, there is a limit on the smallest mode a mesh can still represent, and, unless a Direct Numerical Simulation (DNS) is being employed, the mesh is still bigger than the size where dissipation is strong enough to end the energy cascade. In order to prevent the accumulation of energy in the smallest modes, we thus need to add to the Navier-Stokes equations a dissipative term, which is usually done by modeling the subgrid tensor τ_{sgs} as trace free tensor as:

$$\tau_{sgs\ ij} - \frac{1}{3} \tau_{sgs\ kk} \delta_{ij} = -2 \nu_{sgs} \langle S_{ij} \rangle \quad ; \quad \langle S_{ij} \rangle = \frac{1}{2} \left(\frac{\partial \langle u_i \rangle}{\partial x_j} + \frac{\partial \langle u_j \rangle}{\partial x_i} \right), \quad (13)$$

where ν_{sgs} is the subgrid viscosity, which is the essence of the SGSM.

Another complicating factor when transforming a continuous dynamic system in a discrete one is that, as we go toward the smallest modes supported by the mesh, the relative resolution becomes very poor, to a point where there can be no structures in-between the smallest one and another twice its size.

3.1. Sub-grid Viscosity

In a general external aerodynamic flow, the important turbulence is commonly confined to regions close to the object of interest (airfoil or thin plate in our case) and, in the worst case, may also include a portion of downstream wake. In such high activity locations, regularity on the mesh spacing is desired anyway to guarantee a low "commutative error-subgrid term" ratio, justifying efforts to improve subgrid models (SGSM). Away from this regions, upwind (or other dissipative schemes) can be safely used, since there is no danger of damping turbulence structures.

Therefore the strategy used here consists in defining, based on previous experience or experimental data, a closed region around the flat plate where turbulence is not insignificant and where a central difference scheme is employed together with a high quality mesh. Outside this region, a dissipative scheme allows increasing mesh spacing towards external boundaries, without penalties for the accuracy of turbulence simulations.

Although this strategy is general enough to be used with many combinations of dissipative schemes and SGSM, this paper is restricted to the use of standard upwind scheme along with the one equation SGSM of Horiuti (1985) to model the subgrid viscosity ν_{sgs}

$$\nu_{SGS} = C_{\kappa} \bar{\Delta} \sqrt{\kappa_{sgs}} \quad (14)$$

where the sub-grid length scale is proportional to the mesh size $\bar{\Delta}$ and the sub-grid velocity scale is the subgrid kinetic energy κ_{sgs} , which is obtained from its transport equation

$$\frac{\partial \kappa_{sgs}}{\partial t} + \nabla \cdot (\bar{\mathbf{u}} \kappa_{sgs}) = \nabla \cdot \left[\left(\frac{\mu}{\rho} + \nu_{sgs} \right) \nabla \kappa_{sgs} \right] + G_{\kappa,sgs} - \frac{C_{\varepsilon} \kappa_{sgs}^{3/2}}{\bar{\Delta}} \quad ; \quad G_{\kappa,sgs} = \tau_{sgs\ ij} \langle S_{ij} \rangle \quad (15)$$

In the derivation of Eq. (15) the turbulent transport and the pressure diffusion have been modeled compactly as a diffusion process.

Although standard first-order upwind scheme is known to be too dissipative, its choice was based on the assumption that its active region will be limited by design to that of laminar flow regime, where no important structure is at risk of being damped. The main motivation for the choice of the one equation SGSM, on the other hand, was its ability to deal with non-equilibrium situations, where turbulent production and dissipation do not necessarily balance each other.

If this SGSM represents a step forward in capturing situations where turbulent production and dissipation are not in equilibrium, one of the key issues regarding LES is still untouched, which is extremely important in the present particular case. Indeed, the length scale $\bar{\Delta}$, usually defined as the cubic root of the elementary volume, $\sqrt[3]{V}$ is only reasonable for control volumes whose aspect ratio is close to one. For elongated elements, where aspect ration is important, it proves incapable of representing the complexity of mesh anisotropy, resulting in a viscosity too big for the structures lying in some directions and at the same time too low for structures in other directions.

In the particular case of a external flow over a thin flat plate, the presence of a wall only contributes to further

widen the range of scales, with very small structures in the boundary layer and much bigger ones away from the walls. From the SGS model perspective, this ideally requires a gradual increase in the spanwise mesh spacing away from the wall in its normal direction, which not only increases commutative error, but cannot be obtained with a structured mesh. Therefore it is inevitable that the one equation SGS model overpredicts the eddy-viscosity in some places and underpredicts it in others. Therefore, mesh validation is a very important part of this work.

It must be reinforced that, without this mixed scheme, or in other words, employing pure central-differences over the entire domain, every tentative of simulation ended with number overflow, due to the mentioned mesh-related instability.

4. Results

The flow field was obtained with the free open-source CFD framework called OpenFOAM (Weller et al. 1998), which easily allows new implementations, as the one presented in this paper. It is based on Finite Volume Method, where all the variables are stored at the control volume's centroid, being face-interpolated when needed. PISO algorithm (Issa, 1985) was employed on all simulations, using second order "backward differencing" time step discretization. Unless otherwise specified, all discretization schemes and other details followed exactly version 1.2 of OpenFOAM.

The geometry of the flat plate follows the work of Crompton (2001) and Collie et al (2003) and is shown in Fig. (2). However, since LES is an expensive methodology, it was adopted a smaller computational domain, than the one used by Collie et al (2003). Preliminary investigations of the same problem (Sampaio and Nieckele, 2004) showed that the smaller domain did not present any significant influence to the final solution. Numbered auxiliary regions intended to help mesh elements distribution, are shown in the same Fig. (3). Block number 15 is of particular interest, since it was expected to enclose the whole main bubble, according to Crompton's experiment.

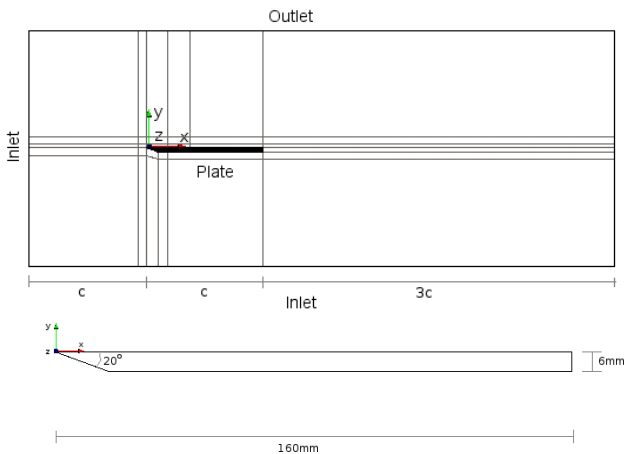


Figure 2. Thin flat plate geometry and domain

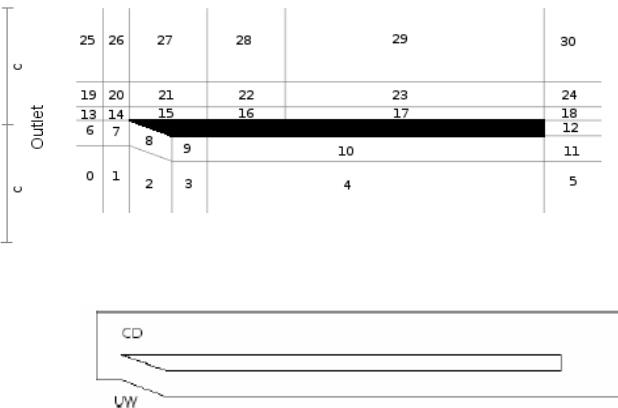


Figure 3. Thin flat plate geometry and auxiliary block

The boundary conditions are also indicated in Fig. (2), and consist of: prescribed velocity, no turbulence kinetic energy and zero pressure gradient in the inlet boundary; zero velocity and turbulence energy gradient and zero pressure in the outlet boundary; zero velocity, zero kinetic energy and zero pressure gradient at the plate walls; and periodic conditions at the z-planes.

Structured meshes were used throughout this work, since they require fewer elements to fill the domain, and potentially present less error due to mesh non-orthogonality.

Aiming to fully understand the mesh requirements and limitations, several mesh distributions were employed. Initially a coarse mesh was specified, which allowed faster computation time and several subsequent runs were performed, with refinements in different directions, so that conclusions could be drawn as to which direction or which refinement were more crucial to the accuracy of the simulations.

A grid test was performed, with a starting mesh for this set of simulations, hereby referenced as 400k mesh, consisting of 418,992 control volumes, being 16 divisions used in the z direction, which spans 1/4th of the chord. For a 16 cm-long plate, the finest control volume, found inside auxiliary block number 15, measures 0.01×0.04×0.25 (Height × Length × Depth) cm, guaranteeing a y^+ below 10 throughout the top surface of the plate. While this is not enough for LES in wall-sensitive flows, where usually the transition and separation occurs somewhere along the surface, in the present case it should not be a problem, since the separation of the boundary layer is dictated by a abrupt curvature -- actually a knife edge - in the geometry, and happens at a well defined point. Transition of the separated shear layer is also shown experimentally to occur very close to the leading edge for Reynolds numbers above 100,000; which means the rest of the flow is also not very sensitive to this.

For the second mesh, the number of divisions in z direction was doubled for the mesh hereby referenced as 800k, while keeping the same wingspan as the 400k mesh. Finally, a third mesh with 1254096 control volumes, called 1200k,

preserves both wingspan and number of z-direction divisions as the 400k mesh, but it greatly improves regularity downstream of the bubble in the x - y plane, particularly along x direction in auxiliary blocks number 16 and 17.

Since the main objective of this study was to capture and to understand the mechanisms inside the bubble, usual mesh recommendations were a bit relaxed in the outer region, so that computational costs were kept at reasonable levels. Therefore, the mesh is designed to be as regular as possible inside the auxiliary block number 15, which measures $0.2 c \times 0.03 c$, where maximum spreading rate was only 0.5%. Therefore, even if some spurious dissipation and inaccurate results are felt downwind of the bubble, one should not expect this to significantly influence the behavior of the simulation inside the bubble.

To be able to obtain a solution, a closed box containing all the expected turbulent structures was defined as shown in Figure (3). In this particular flow, experimental data helped to define this region, but this is rarely the case, since the ultimate goal of simulations is to predict the behavior of the flow, becoming independent of data availability. Inside this box - which contains auxiliary block numbers 7, 8, 9,10, 14, 15, 16 and 17, as well as a small part of blocks 11, 12, and 18 - the central difference schemes was employed, known to be far less dissipative than upwind, which was used everywhere else. However, central difference schemes require the mesh to be as regular as possible to avoid any numerical instability from spurious mesh effects, and this is why the maximum spreading rate was kept as low as 0.5% inside this box.

The fields were initialized from a solution obtained with a simple Spalart-Almaras (1994) RANS model, so that the time consuming evolution towards steady state is shortened. Only after a long enough period of no significant changes in the average variables, the averaging was initialized and the steady-state results began to be computed. In all simulations, time step was chosen so that maximum Courant number was kept below 0.125.

Results from the three meshes are compared in Fig. (4), where mean velocity profiles at 4 stations along the plate are compared to experimental data from Crompton (2001) and RANS k - w model prediction obtained by Collie et al (2003). Although the results inside the main structure for mean velocity profile (Fig. (4a) and (4b) were encouraging with this first mesh, further downstream, excessive dissipation was found, as seen in Fig. (4c) and (4d), where the mean chordwise velocity component profile presented a smooth curvature instead of piecewise-linear like behavior found experimentally. As subgrid viscosity levels were not enough to explain such behavior, two subsequent mesh refinements in different directions were employed aimed to investigate whether this could be attributed to a spurious viscosity, due to an inappropriately large spreading rate.

Inside the bubble, as shown in Fig. (4a) and (4b), one can see that the x - y plane refinement of 1200k mesh did not improve accuracy, while the spanwise refinement (800k) did, specially in the second station, Fig. (4b), located very close to reattachment point. Downstream of the bubble, Fig. (4c) and (4d), all tested meshes failed to provide accurate quantitative results as for-seen, although a slightly better qualitatively result was predicted by 800k mesh, which captured slightly better the piecewise linear trend exhibit by the experiments.

The reattachment lengths for the three meshes tested and for the RANS k - w model used by Collie et al (2003) are shown in Tab. 1, where they are compared to the experimental data from Crompton (2001).

Table 1. Reattachment Lengths

Case	Reattachment Length (% of the chord)	Error relative to Exp. (%)
Exp (Crompton, 2001)	14	-
k - w (Collie et al. 2000)	18.41	24
400k	14.53	3.8
800k	13.95	0.37
1200k	13.25	5.4

The pressure coefficient, defined as

$$c_p = \frac{\langle p \rangle - p_\infty}{\rho U_\infty^2 / 2} , \quad (16)$$

is presented along the top surface at Fig. (5). It reveals that none of the meshes was able to capture the suction on the leading edge of the bubble. Not only is the suction peak lagged in space, as the pressure exhibits an almost linear behavior until it reaches its minimum in the numerical simulations, which is not in agreement with the expected smoothly curved behavior. The fact that the 1200k mesh prediction was closer to experimental data may be an indication that more resolution in the x - y plane is required close to the leading edge of the plate, and this refinement is more effective than the wingspan refinement.

To analyze the flow field, it is convenient to determine the second order statistic components, as

$$R_{ij} = \langle u_i' u_j' \rangle \quad ; \quad u_i' = \langle u_i \rangle - \overline{\langle u_i \rangle} \quad (17)$$

where $\overline{\langle u_i \rangle}$ is the time average of the filtered velocity component.

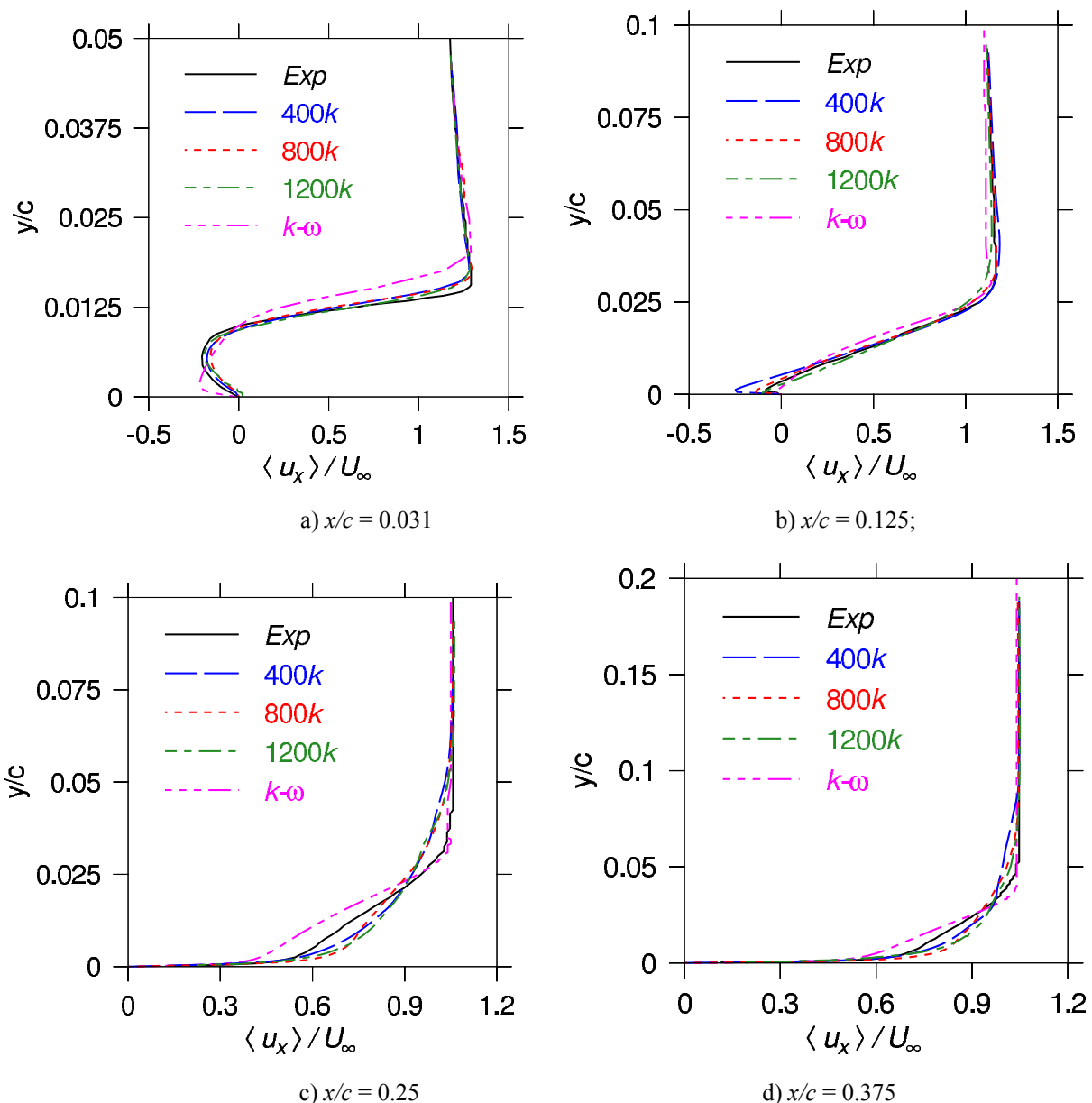


Figure 4. Mean velocity profiles at stations located at: a) $x/c = 0.031$; b) $x/c = 0.125$; c) $x/c = 0.25$; d) $x/c = 0.375$.

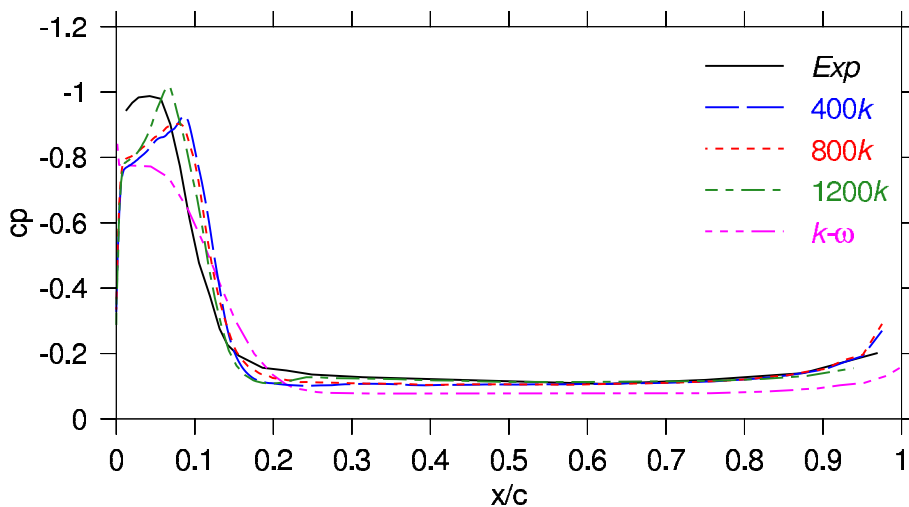


Figure 5. Pressure Coefficient

An analysis of second order turbulent time-statistics, $R_{11} = \langle u' u' \rangle$, at Fig. (6), shows that most of the turbulent kinetic energy is not resolved inside the bubble (station 1). It is also evident that, in the numerical simulations, the maximum of energy happens at station 2, while experiments suggest that the peak should happen earlier, at station 1. A possible explanation for this behavior is that the mesh in this region is too coarse, yielding an excessive dissipation which leaves too much energy to be modeled and delays transition to a complete turbulent regime. It is also worth noticing that the 400k mesh transports too much energy to regions far from the plate in the normal direction, supposed to be turbulent-free, which explains the excessive smoothness of the corresponding velocity profiles there. Although it is reported that experimental set-up suffers from leading-edge fluttering, thus increasing the measured energy, this is not enough to explain the big discrepancies found between numerical and experimental results.

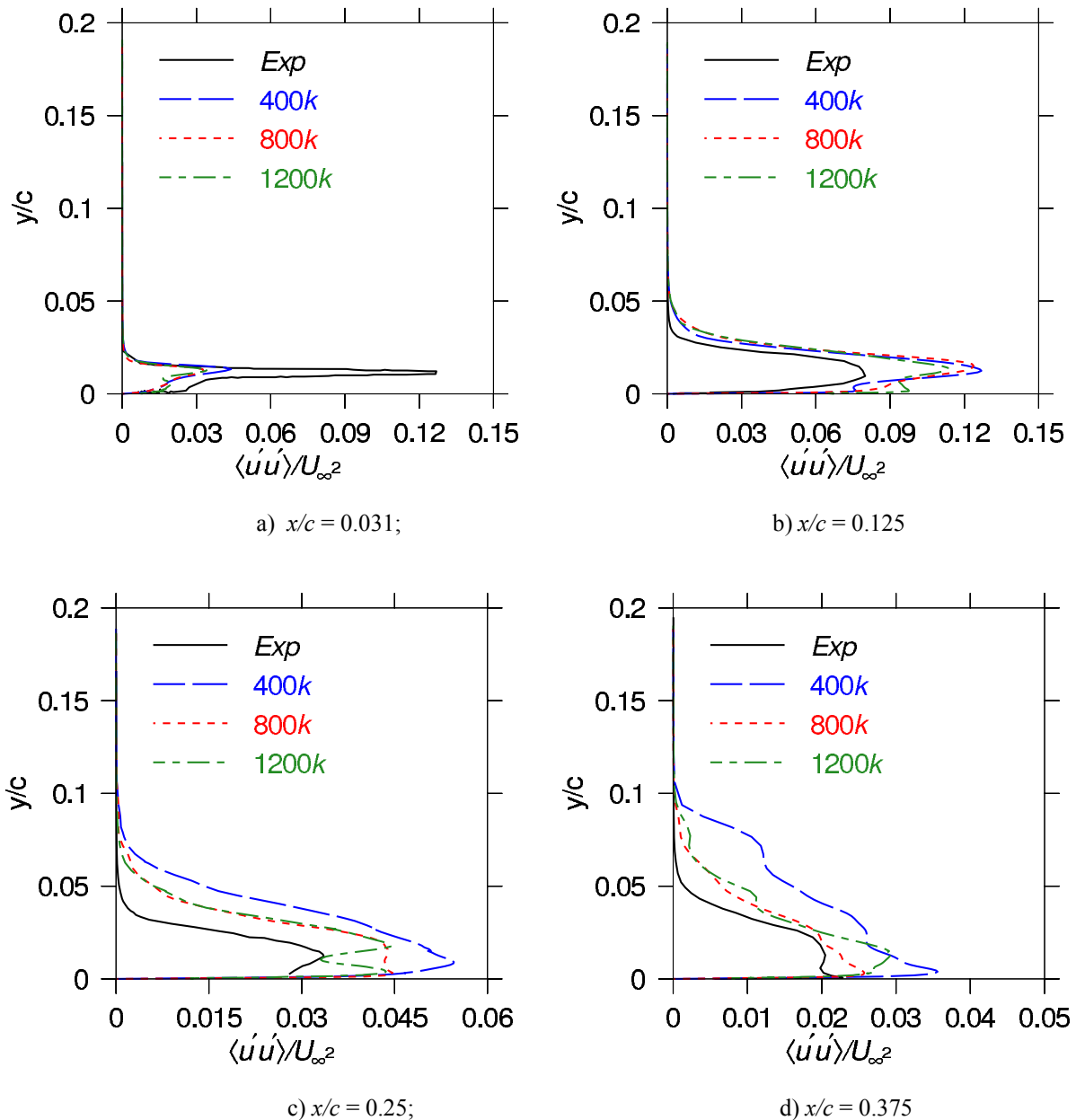


Figure 6. Profiles of second order statistic R_{11} at: a) $x/c = 0.031$; b) $x/c = 0.125$; c) $x/c = 0.25$; d) $x/c = 0.375$

Figure (7) shows a secondary recirculation bubble inside the main one, which is not captured by any tested RANS models (Collie et al., 2003). This secondary bubble is formed after a relaminarization of the boundary layer in its way back to the leading edge, somewhere in-between the minimum pressure region close to the center of the main recirculation and the higher pressure area close to the forward end of the plate. The adverse pressure gradient there, together with the laminar regime of the boundary layer induces a new separation, thus originating the secondary bubble.

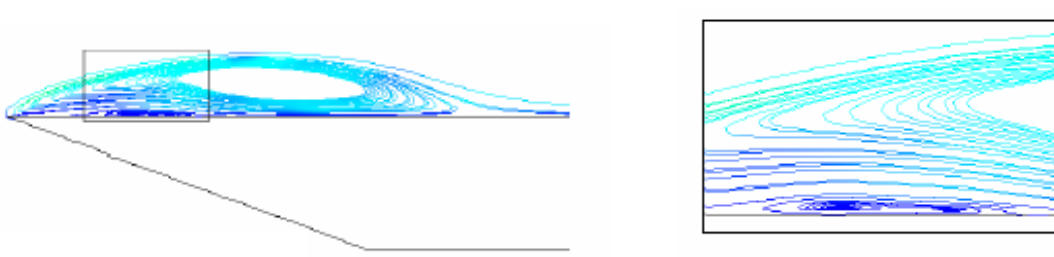


Figure 7. Bubble structure -- Stream traces

One of the reasons why many RANS models fail to capture this structure is their isotropy hypothesis for the turbulent viscosity, which, as we can see from Fig. (8), is not valid at all. It is evident from this same figure that component R_{22} dies much faster than the other two, as wall is approached.

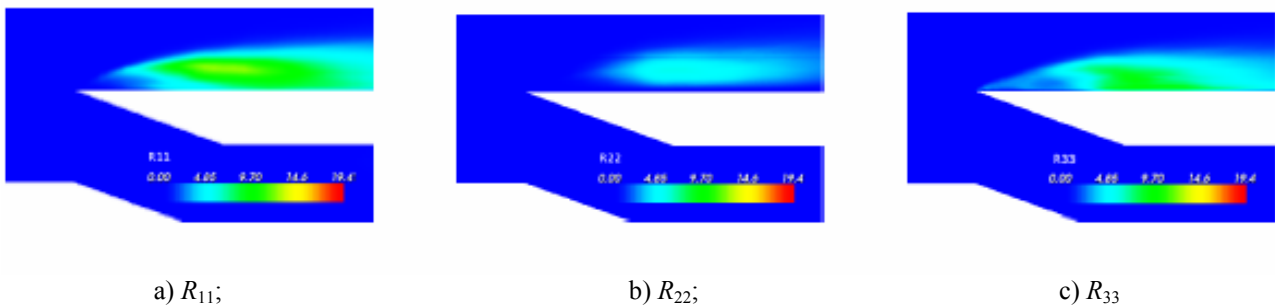


Figure 8. Contours of second order statistics components: a) R_{11} ; b) R_{22} ; c) R_{33}

The second invariant field can be employed to help identify the coherent vertical structures. It can be defined as

$$Q = \frac{1}{2} (\langle S_{ij} \rangle \langle S_{ij} \rangle - \langle \Omega_{ij} \rangle \langle \Omega_{ij} \rangle) \quad (18)$$

where $\langle S_{ij} \rangle$ and $\langle \Omega_{ij} \rangle$ are defined by Eq. (7) based on the filtered velocity.

Figure (9) is a snapshot of the second invariant field, Q , while Fig. (10) presents contours of vorticity magnitude and vortex tubes. One can see at Fig. (9) the initially spanwise rectilinear structures close to the leading edge evolving towards chaotic ones further downwind, in a mechanism known as coherent vortices breakdown.

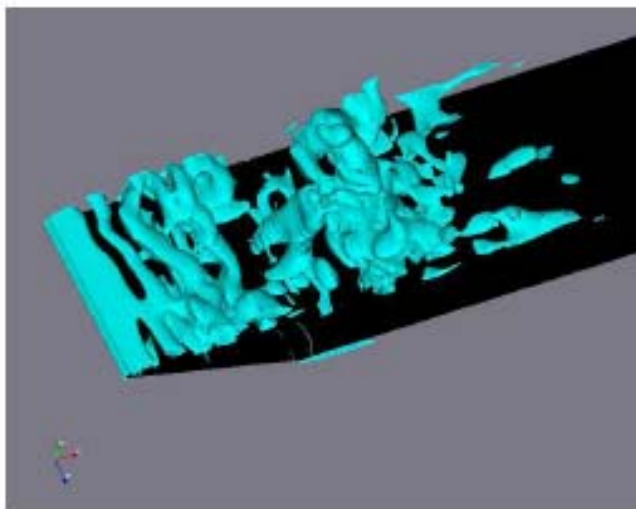


Figure 9. Coherent Vortices according to the Second Invariant criteria.

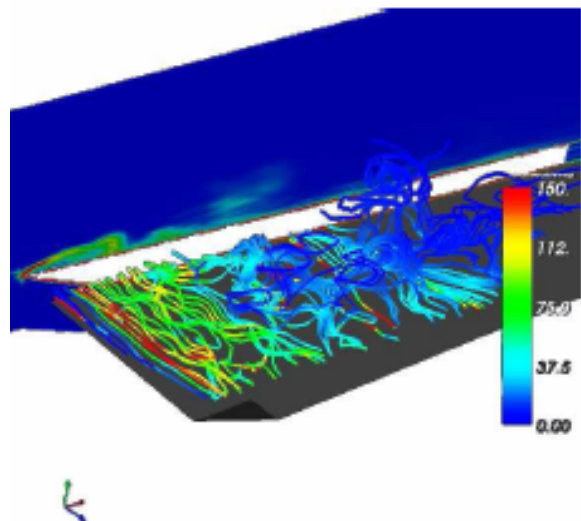


Figure 10. Contours of vorticity magnitude and vortex tubes, colored by vorticity magnitude

It is important to note that, in Fig. (9), what is broken is the coherence of vortical structures according to some criteria - in this case, the Q criteria - and not the vortex tubes, which can only terminate in a boundary. As shown in Fig. (10), these tubes in fact never brake, although they also evolve from rectilinear filaments to more disorganized and bended structures as they are transported by the flow.

5. Conclusions

The comparison of the LES and RANS results for a flow over a flat plate at small incidence showed that although a large computational effort is necessary to obtain the solution with LES, several improvements were obtained. The present LES simulations allowed some interesting conclusions on the physical aspects of the flow. It was possible to discriminate between coherence structures that contribute to the averaged field, like the main leading edge bubble, and the non-coherent eddy structures carried by the principal stream, which cancels out in the average process.

The traditional one-equation sub-grid modeling, commonly used in Large-Eddy Simulation has been employed with a mixed "upwind" and central-differences approach. It was shown that it yields good results, even for relatively course meshes. However, the use of a pure central-differences was not possible in the present investigation, since the mesh shrinking towards the inlet boundary would always lead to simulation blow-out. This mixed approach has the inconvenience, however, of requiring prior knowledge of the flow, its turbulent and laminar zones, which no simulation should rely upon.

Therefore a new approach must be developed, where functionalities of both sub-grid modeling and numerical instability treatment are provided.

6. Acknowledgement

The first two authors acknowledge the support awarded to this research by CNPq, and CAPES, as well as UFES and Stanford University for providing computational resources to help develop the present work.

7. References

- Collie, S., Jackson, P. S., Gerritsen, M., 2003, "Turbulence Modelling Of The Flat Plate At Shallow Incidence", Yacht Research Unit, University of Auckland, Private Bag 92019, Auckland, New Zeland.
- Crompton, M. J., e Barret, R. V., 2001, "Investigation Of The Separation Bubble Formed Behind The Sharp Leading Edge Of A Flat Plate At Incidence", Proc. Instn Mech. Engrs, v. 134 Part G.
- Gault, D.E., 1955, "An experimental investigation of regions of separated laminar flow, report NACA TN.
- Gault, D.E., 1957, "An investigation at low speed of the flow over a simulated flat plate at small angles of attack using pitot static and hot-wire probes, report NACA TN.
- Germano, M, 2000, "On the physical effects of variable filtering lenghts and times in LES", Advances in LES of Complex Flows, Proceedings of the Euromech Colloquium 412, pp. 3-11, editor Friedrich, R and Rodi, W
- Germano, M, 1999, "From RANS to DNS: Towards a Bridging Model", Direct and Large-Eddy Simulation III, Proceedings of the Isaac Newton Institute Symposium, ERCOFTAC workshop, v. 7, pp. 225-236
- Germano, M. and Piomelli, U. and Moin, P. and Cabot, W. H., 1991, "A dynamic subgrid-scale eddy viscosity model", Phys. Fluids A, v. 3, pp.1760-1765.
- Horiuti, K., 1985, Large eddy simulation of turbulent channel flow by one-equation modeling, *J. Phys. Soc.Japan*, Vol. 54, No. 8, pp. 2855-2865.
- Issa, R., 1985, "Solution of the Implicit Discretized Fluid Flow Equations by Operator-Splitting", Journal of Computational Physics, v. 62, pp. 40-65.
- Sagaut, P., 2002, "Large Eddy Simulation for Incompressible Flows, An Introduction", Springer, Second Edition.
- Sampaio, L. E. B, and Nieckele, A. O., 2004, "Large-Eddy Simulation Of The Turbulent Flow Over A Flat Plate At Small Incidence, ETT3, Proceedings of Escola de Primavera de Transição e Turbulência, Porto Alegre, RS, Brasil
- Smagorinsky, J., 1963, General circulation experiments with the primitive equations. I: the basic experiment, *Month Wealth*, Vol. Rev. 91, No. 3, pp. 99-165.
- Spalart, 1994, A one equation turbulence model for aerodynamic flows, *La Recherche Aerospatale*, Vol. 1, pp. 5-21.
- Weller, H., Tabor, G., Jasak, H., and Fureby, C., 1998, A tensorial approach to computational continuum mechanics using object orientated techniques, *Computers in Physics*, Vol. 12, No. 6, pp. 620 - 631.
- Wilcox, D. C., 1988, "Reassessment of The Scale-Determining Equation For Advanced Turbulence Models", *AIAA Journal*, Vol. 26.

8. Copyright Notice

The authors are the only responsible for the printed material included in his paper.